journal

J. Am. Ceram. Soc., **83** [9] 2255–62 (2000)

Model for Cyclic Fatigue of Quasi-Plastic Ceramics in Contact with Spheres

Kee Sung Lee, Yeon-Gil Jung, Irene M. Peterson,* and Brian R. Lawn*

Materials Science and Engineering Laboratory, National Institute of Standards and Technology, Gaithersburg, Maryland 20899

Do Kyung Kim*

Department of Materials Science and Engineering, Korea Advanced Institute of Science and Technology, Yusong, Taejon 305-701, Korea

Seung Kun Lee*

Advanced Materials Technology, Technical Center, Caterpillar Inc., Mossville, Illinois 61656

A model of contact damage accumulation from cyclic loading with spheres and ensuing strength degradation in relatively tough, heterogeneous ceramics is developed. The damage takes the form of a quasi-plastic zone beneath the contact, consisting of an array of closed frictional shear faults with attendant "wing" microcracks at their ends. Contact fatigue takes place by attrition of the frictional resistance at the sliding fault interfaces, in accordance with an empirical degradation law, allowing the microcracks to extend. At large numbers of cycles or loads the microcracks coalesce, ultimately into radial cracks. Fracture mechanics relations for the strength degradation as a function of number of cycles and contact load are derived. Indentation–strength data from two well-studied coarse-grain quasi-plastic ceramics, a micaceous glass-ceramic and a silicon nitride, are used to evaluate the model. Comparative tests in static and cyclic contact loading confirm a dominant mechanical component in the fatigue. At the same time, the presence of water is shown to enhance the fatigue. The model accounts for the broader trends in the strength degradation data, and paves the way for consideration of key variables in microstructural design for optimum fatigue resistance.

I. Introduction

All ceramics fatigue in repeat loading,[1–7] to a greater or lesser extent depending on the microstructure, even in compressive fields.[8–10] Ceramics with heterogeneous microstructures are especially susceptible. Heterogeneous, coarse ceramics tend to show enhanced long-crack toughness, mostly by virtue of grain-facet bridging, and typically exhibit *R*-curves.[11–13] In long-crack tests such materials fatigue primarily by progressive mechanical degradation of frictional tractions at the sliding grain facets behind the advancing crack front.[14–18] Basically, the fatigue diminishes any crack-tip shielding, effectively restoring the material to its untoughened state.

The susceptibility of tough ceramics to fatigue is even more pronounced in contact loading with hard spheres, where inordinately high stress intensities result in progressive local damage accumulation, leading to deleterious reductions in material strength.[19–24] Ceramic engine components, including bearings, and biomechanical structures, such as dental restorations and biomechanical prostheses, are practical examples.[25] The nature of the contact damage in tough ceramics is fundamentally different from that in brittle ceramics.[25,26] In fine, homogeneous structures the damage takes the form of classical macroscopic cone cracks in a region of weak tension outside the contact ("brittle" mode). Strength losses from this damage mode are initially abrupt as the cone cracks pop in, but fall off only slightly thereafter with increasing numbers of cycles—and the degradation is no faster in cyclic than in static contact loading, suggesting a process based purely on time-dependent slow crack growth.[27] In coarser, heterogeneous structures the damage manifests itself as a cloud of closed shear microcracks or "faults" at microstructurally limited weak boundaries within a subsurface shear–compression deformation zone ("quasi-plastic" mode). Strength losses in the initial damage stages are now more gradual, corresponding to failures from individual, small microcracks, but rapidly accelerate with extensive cycling as the microcracks coalesce into dangerous radial cracks. The degradation now depends more strongly on number of cycles than on integrated time in the contact, indicating true mechanical fatigue. In the toughest ceramics the quasi-plastic mode tends to dominate at all stages of the contact damage process.[24] These same tough materials tend also to show accelerated material removal by coalescence of adjacent faults, with consequences relating to wear and machining properties. Interestingly, under extreme contact cycling conditions, quasi-plasticity can manifest itself even in the most homogeneous materials,[24] pointing to an ultimate dominance of this damage mode in all ceramics.

Theoretical analyses of contact-induced strength degradation are only now being realized. A model presented in a preceding paper quantifying strength as a function of indentation load in *single-cycle* contacts provides the basis for such analyses.[28] It is necessary only to incorporate an element accounting for the incremental evolution of damage over each cycle. A contact fatigue model has recently been developed for ideally brittle ceramics,[29] based on the traditional concept of environmentally assisted slow cone-crack growth. Analogous descriptions for quasi-plastic ceramics have been foreshadowed in earlier studies, in which the underlying contact fatigue process is described in terms of mechanical degradation of frictional tractions at sliding

G.M. Pharr—contributing editor

Manuscript No. 189038. Received October 5, 1999; approved February 29, 2000.
This work was funded in part by internal funds from the National Institute for Standards and Technology and in part by grants from the National Institutes for Dental Research and the Korea Science and Engineering Foundation.

* Member, American Ceramic Society.

microstructural shear faults,[30,31] akin to the mechanism of bridging degradation at long cracks. However, the mechanics of cyclic failure from such shear faults in relation to strength degradation, with particular reference to microcrack coalescence, have not been developed.

Accordingly, in this paper we construct a model of contact damage accumulation and strength degradation from cyclic loading with spheres in relatively tough, heterogeneous ceramics. In accordance with experimental procedure we treat the damage evolution in two stages: (i) cyclic contact damage at prescribed loads and environments; (ii) strength degradation of the damaged specimens in fast fracture. The first stage identifies the damage; the second quantifies it. We take the contact to be essentially quasi-plastic, consisting of an array of closed frictional shear faults with attendant "extensile" or "wing" microcracks at their ends. At large numbers of cycles or loads the faults coalesce by microcrack extension, ultimately into radial cracks. Contact fatigue is assumed to take place by cyclic attrition of the frictional resistance at the repeatedly sliding fault interfaces, according to an empirical degradation law. Working relations for the degraded strength in terms of numbers of cycles and contact load are derived. We evaluate our model using data from two well-studied coarse-grain quasi-plastic ceramics, a micaceous glass-ceramic and a silicon nitride. The bulk of our tests are conducted in cyclic loading in air, but comparative tests in the same environment are also conducted in static loading in air, to confirm a dominant mechanical component in the fatigue. Other comparative tests are conducted in water, to demonstrate that chemical interactions are nevertheless still important. Our model, while somewhat phenomenological in its treatment of the micromechanical processes, nonetheless accounts for the broad trends in contact-fatigue strength-degradation data, and allows for consideration of key microstructural variables in design for optimum fatigue resistance.

II. Mechanics of Quasi-Plastic Damage in Hertzian Contact

(1) Quasi-Plastic Damage in Single-Cycle Contact

Consider a quasi-plastic damage zone produced by Hertzian contact with an elastic sphere of radius r at load P over n cycles, followed by tensile loading at stress σ in flexure (Fig. 1(a)). The damage zone consists of an array of intrinsic closed shear faults, characteristic dimension l, spacing D, with extensile wing crack c (Fig. 1(b)). We suppose that the faults are subject to net sliding friction tractions[32–34]

$$\tau_* = \tau_P - \tau_c \tag{1}$$

where τ_P is the resolved component of shear stress from the applied contact field and τ_c is an intrinsic frictional resistance term ("cohesion stress") at the sliding fault interface. (More generally, there is an extra $\mu\sigma_N$ term on the right-hand side of Eq. (1), but we ignore this term here.)[30,32,33] The net shear stress τ_* can be enhanced by either increasing the contact load P (increasing τ_P) or degrading the friction (diminishing τ_c). The macroscopic quasi-plasticity associated with the fault array can be described by a constitutive bilinear elastic–plastic stress–strain relation $\sigma(\varepsilon)$ for a volume element in uniaxial compression:[35]

$$\sigma = E\varepsilon \qquad (\sigma \le Y) \tag{2a}$$

$$\sigma = Y + \alpha(\varepsilon E - Y) \qquad (\sigma \ge Y) \tag{2b}$$

where E is Young's modulus, Y is the uniaxial yield stress, and α is a strain-hardening coefficient ($\alpha = 0$, fully plastic; $\alpha = 1$, fully elastic),[34]

$$Y = 2\tau_c \tag{3a}$$

$$\alpha = 1/(1 + l^3/4D^3) \tag{3b}$$

Equations (2) and (3) are exact for the special case of parallel equisized faults.[34]

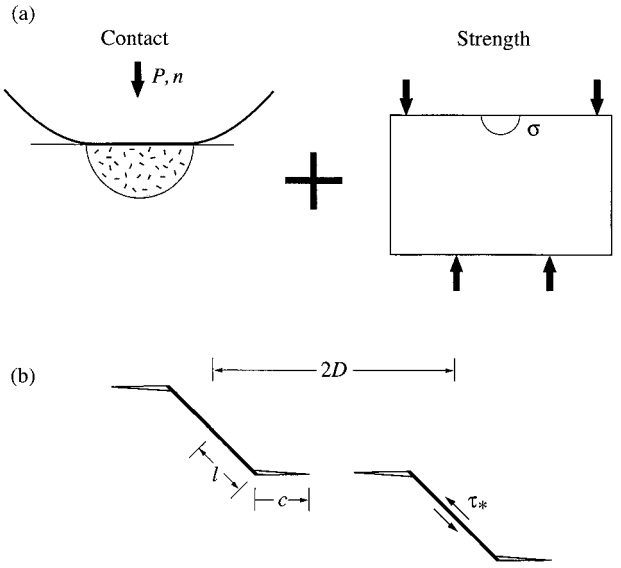

Fig. 1. Model of cyclic strength degradation in quasi-plastic ceramic: (a) Showing two-step indentation–strength sequence. Step 1: Contact at n cycles at load P generates shear faults within quasi-plastic zone. Step 2: Application of bending stress σ takes system to fast failure (inert strength). (b) Coordinates for shear faults with extensile wing cracks. Composite cracks are treated as pennylike with virtual radius $C = c + \gamma l$, with c annular crack dimension and l microstructural fault radius, and mean separation D.

In single-cycle Hertzian contact, deformation is elastic up to a yield load P_Y. Using the Hertzian relation $a^3 = 4kPr/3E$ (Ref. 36) along with a critical stress condition $p_Y = P_Y/\pi a^2 = 1.1Y$ for slip,[37] we have[25]

$$P_Y = (1.1\pi Y)^3(4kr/3E)^2 \tag{4}$$

where $k = (9/16)[(1 - \nu^2) + (1 - \nu'^2)E/E']$ is a dimensionless coefficient, ν is Poisson's ratio, and the prime notation denotes the indenter material. In the plastic region $P \ge P_Y$, an empirical fit to FEM-generated contact stress fields yields an approximate empirical expression for the load dependence of the maximum net sliding stress in the domain $\tau_* \ge 0$, $P \ge P_Y$:[28]

$$\tau_* = \alpha\tau_c[(P/P_Y)^{1/3} - 1] \tag{5}$$

The wing microcracks generated at the ends of the shear faults in Fig. 1(b) during contact are driven by the shear stress τ_*, equivalent to a center-loaded force $Q = \lambda l^2\tau_*$ on a pennylike crack of effective radius $C = c + \gamma l$, with $\gamma = 0.27$.[33,38,39] The equilibrium stress-intensity factor for these cracks is[28]

$$K(C) = \chi Q/C^{3/2} = \chi\lambda l^2\tau_*/C^{3/2} = T_0 \tag{6}$$

where T_0 corresponds to the toughness of the weak internal boundaries in the microstructure. (For now, we ignore any potential terms in Eq. (6) that might be associated with a rising R-curve and the presence of internal stresses.) $K(C)$ persists after the indenter is completely unloaded, because the microcracks are driven by irreversible shear displacements at the fault interfaces.[30]

If the spacing D between neighboring faults is sufficiently small, the cracks may overlap and coalesce at very high contact load, defining a single-cycle "crush" load P_C. The condition for coalescence to occur is that $C = D$, $P = P_C$ in Eq. (6). Combining with Eqs. (3), (4), and (5) yields

$$P_C = (1.1\pi)^3(4kr/3E)^2\{Y + [T_0/\chi\lambda\alpha^{1/2}(1 - \alpha)^{1/2}l^{1/2}]\}^3 \tag{7}$$

Thus P_C increases with increasing grain boundary toughness T_0 and yield stress Y, and with diminishing grain size l (in this context, note that Y may also be an inverse function of l).

(2) Extension to Multicycle Contact

Now consider n repeat contacts at given peak load P (Fig. 1(a)). Attrition in repeat sliding degrades the frictional shear stress τ_c ($\tau_c \propto Y$, Eq. (3*a*)), and hence the contact load P_Y at yield ($P_Y \propto Y^3$, Eq. (4)). Using prime notation to denote repeat loading, we have

$$\tau_{c'} = \beta\tau_c = \beta Y/2 \tag{8a}$$

$$P_{Y'} = \beta^3 P_Y \tag{8b}$$

where the degradation coefficient $\beta = \beta(n)$ is a monotonically declining function, with upper and lower bounds: $\beta = 1$, single-cycle loading limit ($n = 1$); $\beta = 0$, complete degradation limit ($n = N$, say). We may also expect β to decline in some way with resolved stress on the sliding fault,[15] and hence with P.

A simple modification to the indentation stress–strain curve relation in Eq. (5) may then be made by replacing τ_c with $\tau_{c'}$ and P_Y with $P_{Y'}$ from Eq. (8):

$$\tau_{*'} = (\alpha Y/2)[(P/P_Y)^{1/3} - \beta(n)] \tag{9}$$

Note that increasing n (decreasing β) in Eq. (9) increases $\tau_{*'}$, hence increases $K(C)$ in Eq. (6).

The condition for coalescence of adjacent microcracks is again that $C = D$. Inserting Eq. (9) into Eq. (6) and invoking Eq. (7), we obtain the critical condition for coalescence:

$$[(P/P_Y)^{1/3} - \beta(n)]_{C'} = (P_C/P_Y)^{1/3} - 1 \tag{10}$$

From this relation we can determine the critical number of cycles $n_{C'}$ (>1) for crushing at given P or crush load $P_{C'}$ ($<P_C$) at given n, in terms of the single-cycle crush load P_C and yield load P_Y.

(3) Strength Degradation

In this section we determine strength degradation functions $\sigma_F(P)$ at given n and $\sigma_F(n)$ at given P (Fig. 1(a)). The equilibrium stress-intensity factor for the microcrack with the tensile stress σ from the bending field superposed onto the residual-field force Q in Eq. (6) may be written[28]

$$K = \chi Q/C^{3/2} + \psi\sigma C^{1/2} = T_0 \tag{11}$$

This function attains a critical state ($dK/dC = 0$) at $C = C_M$ ($C_M \geq \gamma l$), corresponding to a maximum in $\sigma(C)$ at

$$C_M = (4\chi Q/T_0)^{2/3} = 4^{2/3}C_0 \tag{12}$$

with C_0 the immediate postindentation crack length ($\sigma = 0$).[28] Thus the microcrack undergoes stable extension from C_0 to C_M in the tensile field prior to failure. (Such stable extensions prior to failure are familiar behavior for indentation cracks with residual contact fields.[40]) For large fault separations, $D \geq C_M$, instability is reached before overlap with neighbors can occur—failure is then from a single fault at $C = C_M$, corresponding to a strength $\sigma = \sigma_F = \sigma_M$. For small fault separations, $D < C_M$, coalescence occurs at $C = D$ before any individual fault reaches instability—strength is then determined as $\sigma = \sigma_F$ at $C = D$ in Eq. (11). For very small fault separations, the possibility exists that coalescence will pop in a stable radial crack prior to final instability, in which case failure is determined by the mechanics of radial cracks.[41,42]

We may now specify these strength relations for each of the first two fault-size regions. A convenient boundary condition is $P = P_D$ at $\sigma_F = \sigma_0$, $n = 1$ ($\beta = 1$) in the domain $D \geq C_M$,[28] marking the load P_D ($P_Y \leq P_D \leq P_C$) for the onset of degradation below the natural strength σ_0 from an individual fault in single-cycle loading. From Eqs. (11) and (12), invoking Eqs. (6), (7), and (9), we may write the strength relations in normalized form:

For $\sigma_F \geq S$

$$\sigma_F/\sigma_0 = \{[(P_D/P_Y)^{1/3} - 1]/[(P/P_Y)^{1/3} - \beta(n)]\}^{1/3} \tag{13a}$$

For $\sigma_F \leq S$

$$\sigma_F/\sigma_0 = (4^{4/3}/3)\{[(P_D/P_Y)^{1/3} - 1]/[(P_C/P_Y)^{1/3} - 1]\}^{1/3} \times \{1 - [(P/P_Y)^{1/3} - \beta(n)]/[(P_C/P_Y)^{1/3} - 1]\} \tag{13b}$$

where the stress S ($<\sigma_0$) given by

$$S = 3T_0/4\psi D^{1/2} \tag{14}$$

delineates the crossover point in the two strength functions at $D = C_M$. Note that S is independent of P/P_Y and n in Eq. (14). Of the two strength relations in Eq. (13), that at $\sigma_F \leq S$ is the more rapidly diminishing function of P or n. There is a certain "equivalence" between the variables P and n in Eq. (13); i.e. the same result can be achieved by increasing either P/P_Y or n (decreasing β).

III. Evaluation of Degradation Parameters—Case Studies

(1) Experimental Procedure

In this section we summarize the procedure used to obtain strength degradation data on quasi-plastic ceramics. As case studies, we choose two heterogeneous ceramics whose disposition to quasi-plasticity in contact with spheres has been well documented—a coarse silicon nitride, *C*-Si_3N_4,[23,28,43,44] and a coarse micaceous glass-ceramic, *C*-MGC.[24,35,45,46] Microstructures of these materials are in the form of interconnecting crystalline rods (*C*-Si_3N_4) or platelets (*C*-MGC) in a glassy bonding phase. It is sliding at the weak interphase boundaries that gives rise to the contact quasi-plasticity in these microstructures.[26]

Tests were run on specimens cut to 3 mm × 4mm × 25 mm and polished to 0.5 μm surface finish, with chamfered edges to minimize edge failures. Contact damage was produced by indenting with tungsten carbide (WC) spheres of radius $r = 1.98$ mm (*C*-Si_3N_4) and $r = 3.18$ mm (*C*-MGC), for prescribed cycles n up to 10^7 at frequency $f = 10$ Hz and loads up to $P = 2500$ N (Fig. 1(a)). Inspection of the surface and subsurface contact regions revealed classical quasi-plastic damage zones in these structures, without well-developed cone cracks. Comparative static tests were also made over hold times $t = n/f$, to help isolate any chemical contribution to the damage accumulation. In most cases the tests were conducted in laboratory air, but others were conducted in distilled water to enhance the fatigue effect. Spheres were constantly rotated between tests, to minimize cumulative deformation of the WC, especially on the silicon nitride.[43] Critical loads P_Y for the onset of quasi-plastic damage were measured from surface inspections of contact sites over a range of incrementally increasing loads.

Strength tests were conducted on the bar specimens in 4-point flexure, outer and inner span dimensions 20 mm and 10 mm, with the contact surface on the tensile side. The contact sites were first dried in warm air and covered with a drop of dry silicone oil, and the specimens then broken in fast fracture (<20 ms), to provide "inert strengths." All specimens were examined in a low-power microscope to determine the source of failure, i.e. damage site or "natural" flaw.

(2) Results

Figures 2 and 3 show the surface damage morphology from sphere contacts in *C*-Si_3N_4 and *C*-MGC, at relatively high contact loads (cf. Figs. 4–6 below). Figure 2 compares the morphology for (a) single-cycle and (b) multicycle contacts in air. In both materials the severity of damage is clearly enhanced by the cycling. (Incipient ring cracking is observed in some of these micrographs, but these are only "skin deep."[23,46]) Note the appearance of material removal from the contact zones after multiple contacts, with attendant radial cracking in the *C*-MGC. Figure 3 compares the morphology for contacts over a common test duration: (a) static contacts in air, (b) multicycle contacts in air, and (c) multicycle contacts in water. Comparison of (b) with (a) again reveals enhancement of the damage with cyclic loading in a

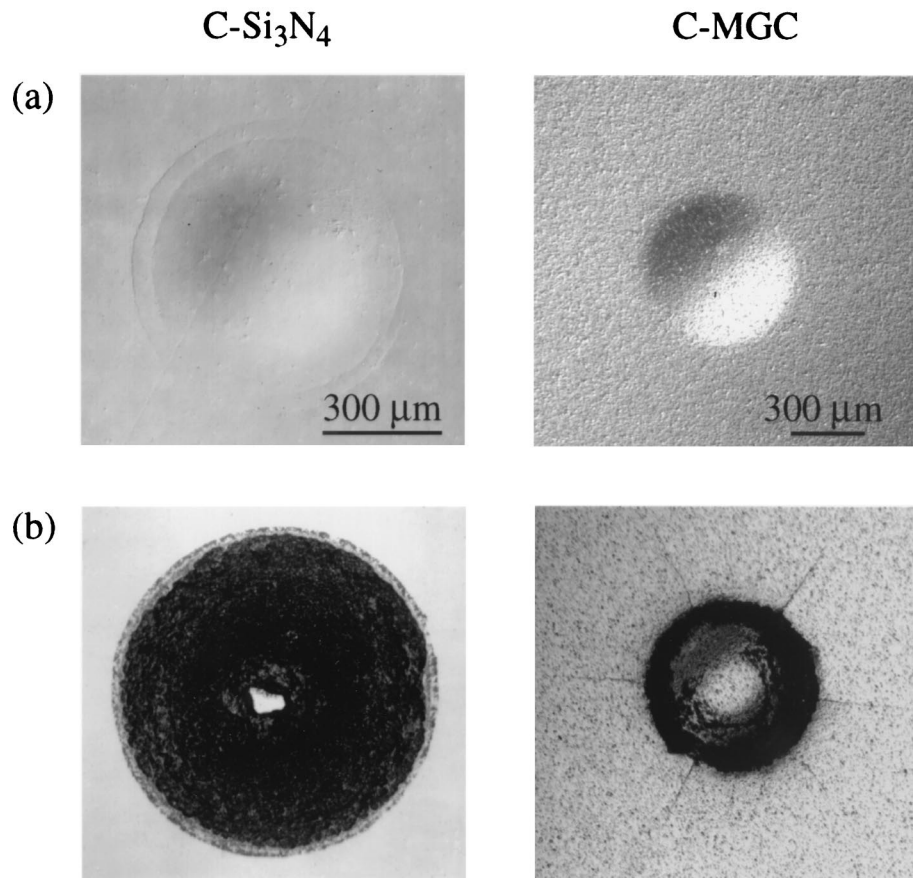

Fig. 2. Optical micrographs of contact sites from indentation with WC spheres, comparing damage in (a) single-cycle and (b) multicycle loading (lower), for tests in air: (left) *C*-Si_3N_4 at $P = 2200$ N, $r = 1.98$ mm, $n = 1$ and 10^7 at $f = 10$ Hz; (right) *C*-MGC at $P = 500$ N, $r = 3.18$ mm, $n = 1$ and 10^6 at $f = 10$ Hz. Surface views, Nomarski contrast, after gold coating.

common air environment, with surface fretting in *C*-Si_3N_4 and radial cracking in *C*-MGC; comparison of (c) with (b) shows further enhancement of this damage from the presence of water, with radial cracking in both materials.

Examination of failure sites in flexure bars containing such damage reveal fracture paths passing characteristically *through* rather than *around* the indentation sites, confirming quasi-plasticity zones as the source of failure.[28,44,46,47] When present, radial cracks provide preferential sites for failure initiation.

Figure 4 plots $\sigma_F(P)$ inert-strength degradation data at numbers of contact cycles n indicated, for sphere contacts on *C*-Si_3N_4 and *C*-MGC in air. Data points are means and standard deviations of a minimum of four specimens. Filled symbols indicate failures from indentation sites—gray symbols from quasi-plastic zones, black symbols from postcontact radial cracks. Unfilled symbols indicate failures from natural flaws. Boxes on the left axes indicate "laboratory" inert strengths (i.e., specimens without indentations). The vertical dashed lines indicate loads for first yield, P_Y, and for first failures from indentation sites, P_D, for $n = 1$ data. Solid curves are fits of the theoretical model to the air environment data, as described in Section III(3). Included as the dashed curves are extrapolations of fits to previous strength degradation data for comparable silicon nitride[43] and glass-ceramic[48] using Vickers indenters, corresponding to failures from well-formed radial cracks. Included as the dashed horizontal lines are the values of evaluated stress S in Eq. (14) (Section III(3)). In the domain of indentation-site failures, the strengths decline steadily with respect to P, more rapidly at higher n. At $\sigma_F < S$, where stress-induced coalescence occurs, the strength falloff is relatively rapid. The data for failures from radial cracks at very large P and n values fall close to the dashed curves, suggesting that the spherical indenters ultimately penetrate and behave as "sharp" indenters.[49]

Figure 5 plots analogous data $\sigma_F(n)$ data at contact loads P indicated, again for sphere contacts on *C*-Si_3N_4 and *C*-MGC in air. At the lower loads in the chosen range, strength losses are observed only above about $n \approx 10^5$–10^7 cycles; at the higher loads, strength losses are observed after just a single cycle, and failures occur universally from indentation sites. Generally, the strength losses begin to accelerate toward the high end of the logarithmic n scale, more rapidly at higher P. Solid curves are again fits of the theoretical model to the air environment data. Again, at $\sigma_F < S$, the strength falloff is relatively rapid.

Figure 6 plots $\sigma_F(n)$ data for sphere contacts on *C*-Si_3N_4 and *C*-MGC, each at a fixed peak load P, for static contact loading in air, cyclic contact loading in air, and contact loading in water. The loads chosen are sufficient to produce failures from indentation origins in all cases. For the tests in air, the strength losses are strongly enhanced in cyclic relative to static contact loading at high n, indicating a strong mechanical component in the fatigue. On the other hand, cycling in water appears to enhance the strength losses relative to those in air, so some chemical effect is also present.

(3) Data Evaluation

Now we fit the theory in Section III(2) to the strength degradation data in Figs. 4–6. For simplicity, we represent $\beta(n)$ by an empirical linear function:[31]

$$\beta(n) = 1 - (n-1)/[N-1] \qquad (0 \le \beta \le 1) \tag{15}$$

where N is the number of cycles to diminish the frictional resistance τ_{cn} in Eq. (8) to zero. In general, we must also expect β to diminish with resolved normal stress on the sliding fault,[15] and hence with P. Again in the interest of simplicity, we propose an empirical relation:

$$N = N_C P_C / P \tag{16}$$

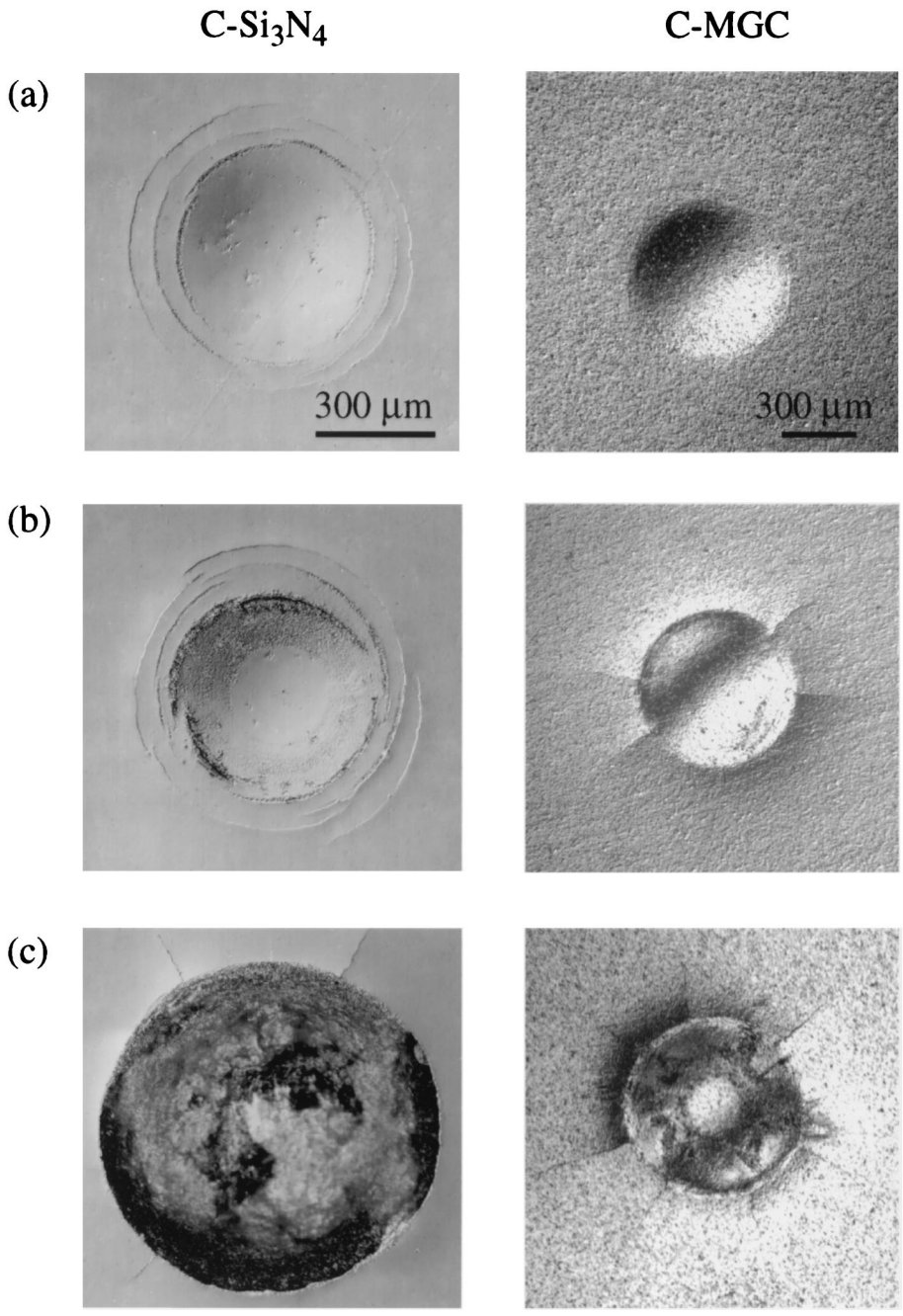

Fig. 3. Optical micrographs of contact sites from indentation with WC spheres, comparing damage from (a) static tests in air, contact duration 10^4 s, (b) cyclic tests at $n = 10^5$ cycles in air at $f = 10$ Hz, and (c) cyclic tests at $n = 10^5$ cycles in water at $f = 10$ Hz: (left) *C*-Si_3N_4 at $P = 2200$ N, $r = 1.98$ mm; (right) *C*-MGC at $P = 500$ N, $r = 3.18$ mm. Surface views, Nomarski contrast, after gold coating.

where N_C is the number of cycles to annul the friction at the single-cycle crush load $P = P_C$. Other, more complex degradation functions are possible.[15]

Several parameters need to be specified in Eqs. (13), (15), and (16). Some parameters are determinable *a priori* by experiments at $n = 1$ in air: natural strength σ_0 (boxes in Figs. 4–6); loads P_D from $\sigma_F(P)$ data, as the loads where failures first occur from indentation sites, and P_Y, from direct measurement of loads for first yield (vertical dashed lines in Fig. 4). This leaves just two adjustable parameters, again pertaining to $n = 1$: crush load P_C, and number of cycles N_C for complete frictional degradation. In our fits we exclude data corresponding to failures away from indentation sites, and from postcontact radial cracks, and include only air-test data. Parameters thus determined are listed in Table I for each material, and appropriate $\sigma_F(P)$ and $\sigma_F(n)$ functions regenerated from Eq. (13) are plotted as the solid curves in Figs. 4–6. The computed stress level S at which σ_F crosses from Eq. (13*a*) to Eq. (13*b*) is indicated in Figs. 4 and 5, indicating the point at which the fault–microcrack coalescence condition is reached during the strength test.

It is seen that the analysis accounts for the broader trends in the cyclic fatigue data in Figs. 4 and 5, notably the accelerated strength degradation at large n and P.

IV. Discussion

We have developed a model of contact fatigue for tough, quasi-plastic ceramics, describing contact damage accumulation from sphere indentation and ensuing strength degradation, with illustrative case studies on a coarse-grain silicon nitride (*C*-Si_3N_4) and micaceous glass-ceramic (*C*-MGC). Our model accounts for the broader features of observed fatigue behavior, most notably the progressive buildup in damage intensity beyond some yield load

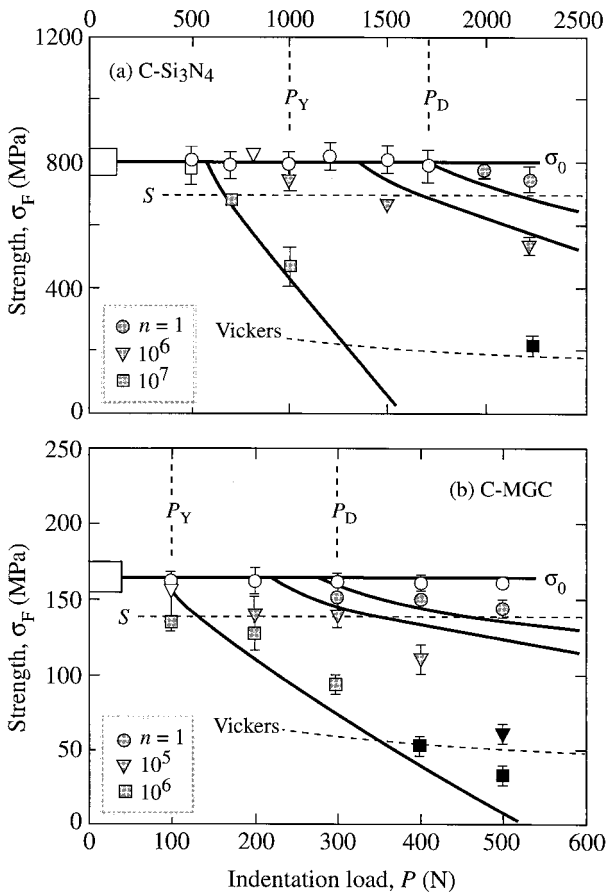

Fig. 4. Inert strength σ_F as a function of peak load P, indentation with WC spheres at number of contact cycles n indicated, $f = 10$ Hz, in air: (a) C-Si_3N_4, $r = 1.98$ mm; and (b) C-MGC, $r = 3.18$ mm. Data points are means and standard deviations, minimum of four specimens per point. Filled symbols indicate failures from indentation sites—gray symbols from quasi-plastic zones, black symbols from preflexure radial cracks. Unfilled symbols indicate failures from natural flaws—box at left axis represents "laboratory" strengths (unindented specimens). Solid curves are theoretical fits to data. Dashed curve corresponds to extrapolation of Vickers data from earlier studies. Vertical dashed lines indicate critical loads P_Y for first yield and P_D for first strength degradation (P_C falls to extreme right of data range). Horizontal dashed line indicates stress S.

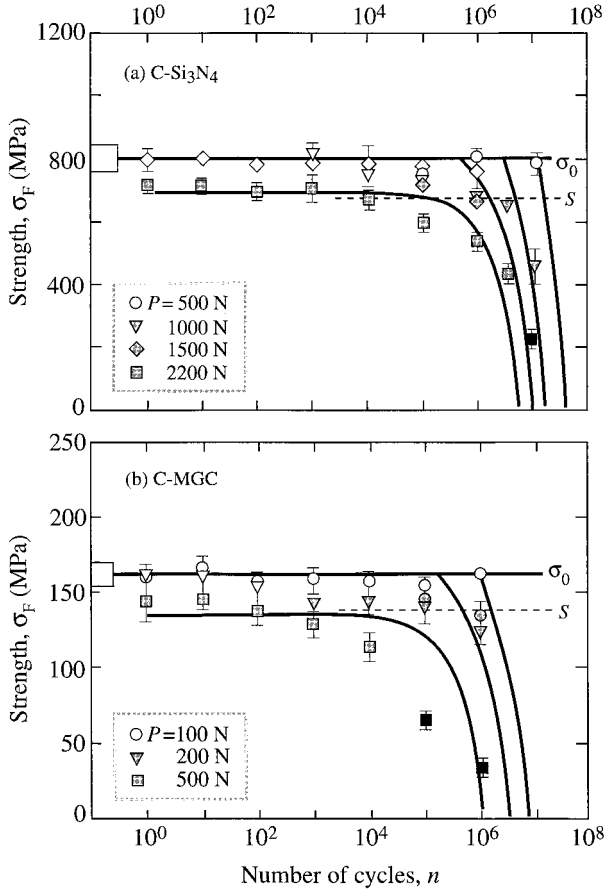

Fig. 5. Inert strength σ_F as a function of number of contact cycles n at $f = 10$ Hz, indentation with WC spheres at maximum loads P indicated, in air: (a) C-Si_3N_4, $r = 1.98$ mm; and (b) C-MGC, $r = 3.18$ mm. Data points are means and standard deviations, minimum of four specimens per point. Filled symbols indicate failures from indentation sites—gray symbols from quasi-plastic zones, black symbols from preflexure radial cracks. Unfilled symbols indicate failures from natural flaws—box at left axis represents "laboratory" strengths (unindented specimens). Solid curves are theoretical fits to data. Dashed curve corresponds to extrapolation of Vickers data from earlier studies. Horizontal dashed line indicates stress S.

P_Y with increasing number of cycles n during contact (Figs. 2 and 3), and a monotonic falloff in ensuing strengths $\sigma_F(P)$ and $\sigma_F(n)$ beyond some threshold contact condition where the shear faults within the quasi-plastic zone exceed the severity of natural flaws, i.e., where failures first occur from the contact sites and σ_F drops below the natural strength level σ_0 (Figs. 4–6). These strength losses accelerate rapidly at high n, highlighting the exceptional vulnerability of quasi-plastic ceramics to fatigue.

Of particular interest in relation to design is the issue of lifetime. From this standpoint, the engineer is most likely to be concerned with the contact conditions for first detectable strength degradation—either a threshold load $P_{D'}$ ($< P_D$) at given n (Fig. 4), or a threshold $n_{D'}$ at given P (Fig. 5) (recalling that prime notation corresponds to $n > 1$). The latter quantity may be derived by inserting $\sigma_F = \sigma_0$ in Eq. (13*a*) and combining with Eqs. (15) and (16):

$$n_{D'} = 1 + (N_C P_C/P - 1)[(P_D/P_Y)^{1/3} - (P/P_Y)^{1/3}] \quad (17)$$

A plot of $n_{D'}(P)$ is given in Fig. 7, using parameters for each material from Table I. This plot may be regarded as a "design map" for a specified set of contact conditions (here for tests with specified WC sphere radius, in air), in which the domain to the lower left of each curve denotes the zone of "safe" operation, i.e., where laboratory strengths are preserved. Note that at $n = 1$ the curves in Fig. 7 tend to the limit $P = P_D$, as required.

Our analysis defines the conditions for the onset of microcrack coalescence during contact and ensuing strength testing, in terms of material parameters. Such coalescence accelerates wear and comminution, as well as strength degradation. One useful parameter is the critical load P_C for coalescence during single-cycle contact (Eq. (7)), and the dependence of the corresponding function $P_{C'}(n)$ for multicycle loading (Eq. (10)). In the special context of strength, a more interesting parameter is $S(D)$ in Eq. (14), here rewritten in terms of grain size l (Fig. 1(b)),

$$S = (3T_0/4\psi l^{1/2})(l/D)^{1/2} \quad (18)$$

corresponding to the applied stress at which coalescence of contact-induced microcracks occurs during postcontact flexure. This quantity establishes the scale of the curves in Figs. 4–6 along the strength axis. For self-similar microstructures (l/D = constant), S is inversely proportional to the square root of l, reminiscent of a Petch relationship[44,46,50] and confirming that susceptibility to quasi-plasticity may be reduced by refining the microstructure. Inverse grain-size dependencies of this kind in the quasi-plastic domain have been experimentally demonstrated elsewhere for Si_3N_4 and MGC materials.[44,46,50] For microstructures with near-contiguous weak-phase structures ($D \approx l$), again typical of our Si_3N_4 and MGC materials, Eq. (18) reduces to $S \approx T_0/\psi l^{1/2}$, i.e.,

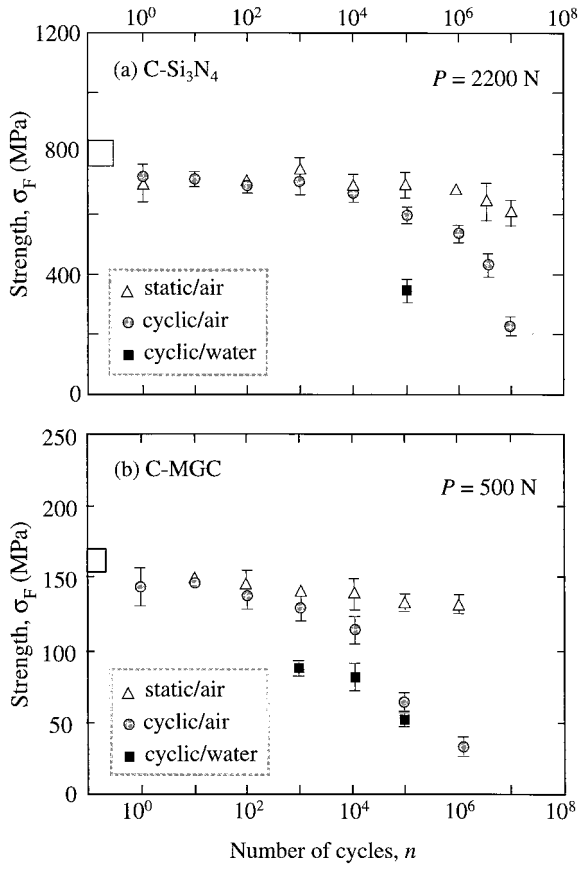

Fig. 6. Inert strength σ_F as a function of number of contact cycles n at f = 10 Hz, indentation with WC spheres, comparing static contact tests (equivalent $n = tf$) in air, cyclic contact tests in air, and cyclic contact tests in water: (a) *C*-Si_3N_4, P = 2200 N, r = 1.98 mm; and (b) *C*-MGC, P = 500 N, r = 3.18 mm. Data points are means and standard deviations, minimum of four specimens per point. All data represent failures from indentation sites.

Table I. Fracture Parameters for Quasi-Plastic Ceramics

Material	σ_0 (MPa)	P_Y (N)	P_D (N)	P_C (N)	N_C
C-Si_3N_4	792	1000	1700	10000	$10^{6.2}$
C-MGC	159	100	300	7000	$10^{4.5}$

in the vicinity of expected natural strengths for failure from grain-boundary-scale flaws. This would explain why S lies just below σ_0 for our materials in Figs. 4 and 5. Conversely, for microstructures with dilute concentrations of shear-faults ($D \gg l$), such that coalescence is no longer a factor in the fatigue failure process, we predict $S \ll \sigma_0$.

It is to be acknowledged that our model, based as it is on a highly idealized shear-fault/extensile-crack configuration (Fig. 1(b)), is phenomenological, notwithstanding considerable precedent for such configurations in the literature.[30,32–34,38,39,51–53] Whereas the formation of well-defined surface radial cracks from microcrack sources within a subsurface quasi-plastic zone is well documented in Vickers indentation studies,[54] there are several questions that may be raised in connection with fine details of the associated micromechanics: (i) Is coalescence a truly physical connection of neighboring microcracks, as implied here, or does it involve some more complex form of nearest-neighbor interaction in the stress-intensity factor? (ii) What is the role of field fluctuations and stochastics in the microcrack populations?[30,39] (iii) What role does residual stress from the integrated microfault population play in driving these radial cracks, as it demonstrably does in Vickers indentations[54] (dashed curves in Figs. 4 and 5)?

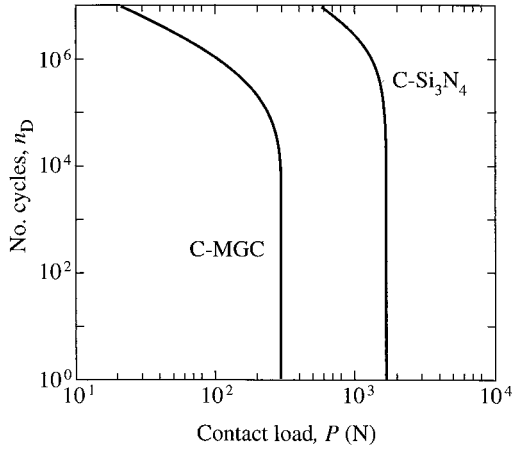

Fig. 7. Plots of number of cycles n_D, as a function of contact load P to induce first detectable strength degradation in *C*-Si_3N_4 and *C*-MGC. Data for r = 1.98 mm (Si_3N_4) and 3.18 mm (MGC).

(iv) We have ignored *R*-curves and internal thermal expansion anisotropy stresses in the current analysis. What is the role of these factors in first driving individual microcracks and then pinning the subsequently coalesced (radial) macrocracks as grain bridging comes into play? (v) What is the physical meaning of the quantity N used to quantify total frictional degradation at the closed shear interfaces? Our linear empirical degradation relation in Eqs. (1), (15), and (16) may be better replaced by some physical wear law,[15] with due allowance for an extra $\mu\sigma_N$ term on the right-hand side of Eq. (1), although at the expense of mathematical simplicity.

Another important issue given only brief attention here is the role of chemistry in the contact fatigue process. In ostensibly brittle solids, glasses, and fine-grain ceramics, where the principal contact damage takes the form of well-defined macroscopic cone cracks, the fatigue is ascribable to slow crack growth from environmental water.[29] In such cases lifetimes in subsequently applied stress fields can be calculated from time-integration of a crack velocity function, a manifestation of which is near-identical $\sigma_F(n)$ functions in cyclic and static contact loading. In the present quasi-plastic ceramics, comparison of cyclic and static data in Fig. 6 shows a much greater strength degradation in cyclic contact loading, indicating a dominant mechanical effect. However, cyclic data in the same figure show an enhanced susceptibility to strength degradation in water than in air, indicating that the presence of water in the contact area does enhance the cyclic fatigue effect. What is the role of water in such cases? Is it to lubricate sliding faces at the closed shear faults, e.g., by increasing hydraulic pressure within interconnecting microcracks,[55,56] thereby progressively reducing the frictional resistance? Or is it to enhance microcrack extension from the ends of the shear faults?[57] In this context we note that whereas the quasi-plasticity process has its origins below the indenter,[19] the access of water is necessarily limited to those microcracks that intersect the top surface outside the contact, signaling a shift in damage accumulation from subsurface to surface.

Finally, the question arises as to what microstructures are most likely to provide optimal resistance to fatigue in ceramics for applications in concentrated loads, as for instance in bearings[23,43,44] and dental ceramics.[24,47] Both "brittle" and "quasi-plastic" modes of damage are deleterious in cyclic fatigue, quasi-plastic especially so because of rapidly accelerating microcrack coalescence at large n or P. (Note that even the most brittle ceramics ultimately degrade by a quasi-plastic mode at sufficiently large n.[29]). In many cases, it appears that the greatest resistance to fatigue comes from "semibrittle" materials, i.e., intermediate microstructures, with enough quasi-plasticity to negate some of the brittleness but not too much as to allow for microdamage coalescence. This tendency to superior performance of "compromise" microstructures has been demonstrated in Si_3N_4[23,43,44] and MGC[46] ceramics.

References

[1]T. Kawakubo and K. Komeya, "Static and Cyclic Fatigue Behavior of a Sintered Silicon Nitride at Room Temperature," *J. Am. Ceram. Soc*., **70** [6] 400–405 (1987).

[2]M. Masuda, T. Soma, M. Matsui, and I. Oda, "Cyclic Fatigue of Sintered Silicon Nitride," *Ceram. Eng. Sci. Proc*., **9** [9–10] 1371–82 (1988).

[3]R. O. Ritchie, "Mechanisms of Fatigue Crack Propagation in Metals, Ceramics, Composites: Role of Crack-Tip Shielding," *Mater. Sci. Eng*., **A103,** 15–28 (1988).

[4]M. Reece, F. Guiu, and M. F. R. Sammur, "Cyclic Fatigue Crack Propagation in Alumina Under Direct Tension—Compression Loading of High-Purity Alumina in Fluid Environments," *J. Am. Ceram. Soc*., **72** [2] 348–52 (1989).

[5]M. Masuda, T. Soma, and M. Matsui, "Cyclic Fatigue Behavior of Sintered Silicon Nitride Ceramics," *J. Eur. Ceram. Soc*., **6** [4] 253–58 (1990).

[6]F. Guiu, M. Reece, and D. A. J. Vaughan, "Cyclic Fatigue of Ceramics," *J. Mater. Sci*., **26** [12] 3275–86 (1991).

[7]R. O. Ritchie, "Mechanisms of Fatigue Crack Propagation in Ductile and Brittle Solids," *Int. J. Fract*., **100** [1] 55–83 (1999).

[8]L. Ewart and S. Suresh, "Crack Propagation in Ceramics Under Cyclic Loads," *J. Mater. Sci*., **22,** 1173–92 (1987).

[9]S. Suresh and J. R. Brockenbrough, "Theory and Experiments of Fracture in Cyclic Fatigue Compression: Single Phase Ceramics, Transforming Ceramics and Ceramic Composites," *Acta Metall*., **36** [6] 1455–70 (1988).

[10]S. Suresh, *Fatigue of Materials.* Cambridge University Press, Cambridge, U.K., 1991.

[11]R. Knehans and R. Steinbrech, "Memory Effect of Crack Resistance During Slow Crack Growth in Notched Al_2O_3 Bend Specimens," *J. Mater. Sci. Lett*., **1** [8] 327–29 (1982).

[12]P. L. Swanson, C. J. Fairbanks, B. R. Lawn, Y.-W. Mai, and B. J. Hockey, "Crack-Interface Grain Bridging as a Fracture Resistance Mechanism in Ceramics: I, Experimental Study on Alumina," *J. Am. Ceram. Soc*., **70** [4] 279–89 (1987).

[13]R. W. Steinbrech, A. Reichl, and W. Schaarwächter, "*R*-Curve Behavior of Long Cracks in Alumina," *J. Am. Ceram. Soc*., **73** [7] 2009–15 (1990).

[14]S. Lathabai, J. Rödel, and B. R. Lawn, "Cyclic Fatigue from Frictional Degradation at Bridging Grains in Alumina," *J. Am. Ceram. Soc*., **74** [6] 1340–48 (1991).

[15]R. H. Dauskardt, "A Frictional Wear Mechanism for Fatigue-Crack Growth in Grain Bridging Ceramics," *Acta Metall. Mater*., **41** [9] 2765–81 (1993).

[16]D. S. Jacobs and I-W. Chen, "Mechanical and Environmental Factors in the Cyclic and Static Fatigue of Silicon Nitride," *J. Am. Ceram. Soc*., **77** [5] 1153–61 (1994).

[17]C. J. Gilbert, R. H. Dauskardt, and R. O. Ritchie, "Behavior of Cyclic Fatigue Cracks in Monolithic Silicon Nitride," *J. Am. Ceram. Soc*., **78** [9] 2291–300 (1995).

[18]J. F. Bartolomé, J. Requena, J. S. Moya, M. Li, and F. Guiu, "Cyclic Fatigue Crack Growth Resistance of Al_2O_3–Al_2TiO_5 Composites," *Acta Mater*., **44** [4] 1361–70 (1996).

[19]F. Guiberteau, N. P. Padture, H. Cai, and B. R. Lawn, "Indentation Fatigue: A Simple Cyclic Hertzian Test for Measuring Damage Accumulation in Polycrystalline Ceramics," *Philos. Mag. A,* **68** [5] 1003–16 (1993).

[20]H. Cai, M. A. S. Kalceff, B. M. Hooks, B. R. Lawn, and K. Chyung, "Cyclic Fatigue of a Mica-Containing Glass-Ceramic at Hertzian Contacts," *J. Mater. Res*., **9** [10] 2654–61 (1994).

[21]N. P. Padture and B. R. Lawn, "Contact Fatigue of a Silicon Carbide with a Heterogeneous Grain Structure," *J. Am. Ceram. Soc*., **78** [6] 1431–38 (1995).

[22]A. Pajares, F. Guiberteau, B. R. Lawn, and S. Lathabai, "Hertzian Contact Damage in Magnesia-Partially-Stabilized Zirconia," *J. Am. Ceram. Soc*., **78** [4] 1083–86 (1995).

[23]S. K. Lee and B. R. Lawn, "Contact Fatigue in Silicon Nitride," *J. Am. Ceram. Soc*., **82** [5] 1281–88 (1999).

[24]Y.-G. Jung, I. M. Peterson, D. K. Kim, and B. R. Lawn, "Lifetime-Limiting Strength Degradation from Contact Fatigue in Dental Ceramics," *J. Dent. Res*., **79** [2] 722–31 (2000).

[25]B. R. Lawn, "Indentation of Ceramics with Spheres: A Century After Hertz," *J. Am. Ceram. Soc*., **81** [8] 1977–94 (1998).

[26]B. R. Lawn, N. P. Padture, H. Cai, and F. Guiberteau, "Making Ceramics 'Ductile'," *Science*, **263**, 1114–16 (1994).

[27]A. G. Evans and E. R. Fuller, "Crack Propagation in Ceramic Materials Under Cyclic Loading Conditions," *Metall. Trans*., **5** [1] 27–33 (1974).

[28]B. R. Lawn, S. K. Lee, I. M. Peterson, and S. Wuttiphan, "A Model of Strength Degradation from Hertzian Contact Damage in Tough Ceramics," *J. Am. Ceram. Soc*., **81** [6] 1509–20 (1998).

[29]D. K. Kim, Y.-G. Jung, I. M. Peterson, and B. R. Lawn, "Cyclic Fatigue of Intrinsically Brittle Ceramics in Contact with Spheres," *Acta Mater*., **47** [18] 4711–25 (2000).

[30]B. R. Lawn, N. P. Padture, F. Guiberteau, and H. Cai, "A Model for Microcrack Initiation and Propagation Beneath Hertzian Contacts in Polycrystalline Ceramics," *Acta Metall*., **42** [5] 1683–93 (1994).

[31]N. P. Padture and B. R. Lawn, "Fatigue in Ceramics with Interconnecting Weak Interfaces: A Study Using Cyclic Hertzian Contacts," *Acta Metall*., **43** [4] 1609–17 (1995).

[32]H. Horii and S. Nemat-Nasser, "Compression-Induced Microcrack Growth in Brittle Solids: Axial Splitting and Shear Failure," *J. Geophys. Res*., **90** [B4] 3105–25 (1985).

[33]H. Horii and S. Nemat-Nasser, "Brittle Failure in Compression: Splitting, Faulting and Brittle-Ductile Transition," *Philos. Trans. R. Soc. London*, **319** [1549] 337–74 (1986).

[34]B. R. Lawn and D. B. Marshall, "Nonlinear Stress–Strain Curves for Solids Containing Closed Cracks with Friction," *J. Mech. Phys. Solids*, **46** [1] 85–113 (1998).

[35]A. C. Fischer-Cripps and B. R. Lawn, "Indentation Stress–Strain Curves for "Quasi-Ductile" *Ceramics," Acta Mater*., **44** [2] 519–27 (1996).

[36]K. L. Johnson, *Contact Mechanics.* Cambridge University Press, London, U.K., 1985.

[37]D. Tabor, *Hardness of Metals.* Clarendon, Oxford, U.K., 1951.

[38]J. M. Kemeny and N. G. W. Cook, "Micromechanics of Deformation in Rock"; pp. 287–311 in *Toughening Mechanisms in Quasi-Brittle Materials.* Edited by S. P. Shah. Kluwer Academic Publishers, Dordrecht, The Netherlands, 1991.

[39]A. V. Dyskin, R. J. Jewell, H. Joer, E. Sahouryeh, and K. B. Ustinov, "Experiments on 3-D Crack Growth in Uniaxial Compression," *Int. J. Fract*., **65** [4] R77–83 (1994).

[40]B. R. Lawn, *Fracture of Brittle Solids*; Ch. 8. Cambridge University Press, Cambridge, U.K., 1993.

[41]D. B. Marshall and B. R. Lawn, "Residual Stress Effects in Sharp-Contact Cracking: I. Indentation Fracture Mechanics," *J. Mater. Sci*., **14** [8] 2001–12 (1979).

[42]D. B. Marshall, B. R. Lawn, and P. Chantikul, "Residual Stress Effects in Sharp-Contact Cracking: II. Strength Degradation," *J. Mater. Sci*., **14** [9] 2225–35 (1979).

[43]S. K. Lee, S. Wuttiphan, and B. R. Lawn, "Role of Microstructure in Hertzian Contact Damage in Silicon Nitride: I, Mechanical Characterization," *J. Am. Ceram. Soc*., **80** [9] 2367–81 (1997).

[44]S. K. Lee and B. R. Lawn, "Role of Microstructure in Hertzian Contact Damage in Silicon Nitride: II, Strength Degradation," *J. Am. Ceram. Soc*., **81** [4] 997–1003 (1998).

[45]D. G. Grossman, "Structure and Physical Properties of Dicor/MGC Glass-Ceramic"; pp. 103–15 in *Proceedings of the International Symposium on Computer Restorations.* Edited by W. H. Mörmann. Quintessence Publishing Co., Chicago, IL, 1991.

[46]I. M. Peterson, S. Wuttiphan, B. R. Lawn, and K. Chyung, "Role of Microstructure on Contact Damage and Strength Degradation of Micaceous Glass-Ceramics," *Dent. Mater*., **14,** 80–89 (1998).

[47]I. M. Peterson, A. Pajares, B. R. Lawn, V. P. Thompson, and E. D. Rekow, "Mechanical Characterization of Dental Ceramics Using Hertzian Contacts," *J. Dent. Res*., **77** [4] 589–602 (1998).

[48]C. J. Fairbanks, B. R. Lawn, R. F. Cook, and Y.-W. Mai, "Microstructure and the Strength of Ceramics"; pp. 23–37 in *Fracture Mechanics of Ceramics*, Vol. 8. Edited by R. C. Bradt, A. G. Evans, D. P. H. Hasselman, and F. F. Lange. Plenum, New York, 1986.

[49]B. R. Lawn and T. R. Wilshaw, "Indentation Fracture: Principles and Applications," *J. Mater. Sci*., **10** [6] 1049–81 (1975).

[50]A. C. Fischer-Cripps and B. R. Lawn, "Stress Analysis of Contact Deformation in Quasi-Plastic Ceramics," *J. Am. Ceram. Soc*., **79** [10] 2609–18 (1996).

[51]M. F. Ashby and S. D. Hallam, "The Failure of Brittle Solids Containing Small Cracks Under Compressive Stress States," *Acta Metall. Mater*., **34** [3] 497–510 (1986).

[52]C. G. Sammis and M. F. Ashby, "The Failure of Brittle Porous Solids Under Compressive Stress States," *Acta Metall*., **34** [3] 511–26 (1986).

[53]L. R. Myer, J. M. Kemeny, Z. Zheng, R. Suarez, R. T. Ewy, and N. G. W. Cook, "Extensile Cracking in Porous Rock Under Differential Compressive Stress," *Appl. Mech. Rev*., **45** [8] 263–80 (1992).

[54]B. R. Lawn, A. G. Evans, and D. B. Marshall, "Elastic/Plastic Indentation Damage in Ceramics: The Median/Radial Crack System," *J. Am. Ceram. Soc*., **63** [9–10] 574–81 (1980).

[55]J. C. Jaeger and N. G. W. Cook, *Fundamentals of Rock Mechanics*; Ch. 8. Chapman and Hall, London, U.K., 1971.

[56]K. S. Yi, S. J. Dill, and R. H. Dauskardt, "Subcritical Crack Growth in Glasses Under Cyclic Loads: Effect of Hydrodynamic Pressure in Aqueous Environments," *Acta Mater*., **45** [7] 2671–84 (1997).

[57]S. Lathabai, J. Rödel, B. R. Lawn, and T. P. Dabbs, "Fracture Mechanics Model for Subthreshold Indentation Flaws: II, Nonequilibrium Fracture," *J. Mater. Sci*., **26,** 2313–21 (1991). □